Wavelength-Multiplexed Polymer LEDs: Towards 55 Mb/s Organic Visible Light Communications

Paul Anthony Haigh, Francesco Bausi, Hoa Le Minh, Ioannis Papakonstantinou, Wasiu O. Popoola, Andrew Burton, and Franco Cacialli

***Abstract*—We present recent progress on visible light communication systems using polymer light-emitting diodes as the transmitters and a commercial silicon photodetector as the receiver. In this paper, we use transmitters at red, green, and blue wavelengths to investigate the maximum on-off keying link performance of each device type as the first steps toward a wavelength-division multiplexed link. We show that a total transmission speed of 13 Mb/s is achievable when considering the raw bandwidth of each of the RGB PLEDs. Such a rate represents a 30% gain over previously demonstrated systems. Further capacity improvement can be achieved using high performance artificial neural network equalizer offering a realistic prospect for transmission speeds up to 54.9 Mb/s.**

***Index Terms*—Equalizers, organic light-emitting diodes, polymer light-emitting diodes, visible light communications.**

I. Introduction

POLYMER light-emitting diodes (PLEDs) offer remarkable potential for low-cost, large active area lighting panels and displays. Such is the promise of PLEDs and polymer electronics that the sector has a projected value of $330 billion as early as 2027; more than the silicon electronics sector is worth today [1]. One of the major reasons for this is the ability to dissolve polymers into solutions and process arbitrarily-shaped panels with methods such as spray-coating or inkjet printing at room temperature.

Concurrently, visible light communication (VLC) has been proposed as a promising candidate as the solution for the so-called last-meter bottleneck caused by an exponentially increasing user demand for data [2]. This is because of a variety of key advantages, and especially because of a huge, unregulated ~400 THz bandwidth free of licensing costs which is currently under-utilized. Furthermore, since light is confined by opaque objects such as walls, VLC offers a higher level of security in comparison to radio frequency technologies. It is envisaged that VLC applications can be grouped into several broad categories; (*i*) future smart homes/offices providing ubiquitous broadcasting networks and room illumination; (*ii*) hospitals and aircraft applications, where currently radio frequency technologies cannot operate due to critical interference with important frequencies; (*iii*) transport networks providing intelligent automated braking and accurate positioning systems, and, finally (*iv*) mobile device-to-device communications with VLC transceivers embedded into the screens and chassis.

For cases (*i*), (*ii*), and (*iii*) semiconductor light-emitting diodes (LEDs) and photodetectors have been commonly adopted as the optoelectronic devices due to high optical power and wide bandwidths. However, there is an increasingly convincing argument to seek alternative devices for case (*iv*). Mobile device and display manufacturers are increasingly moving toward matrices of small-molecule organic LEDs (SMOLEDs) to replace liquid crystal displays (LCDs). While LCDs are cheap, their temporal response is in the region of milliseconds; hence their bandwidths are not suitable for communications purposes. They are not natural displays either, and have a requirement for inorganic LED backlights and color filters. SMOLEDs on the other hand are natural sources of light that can easily be patterned into displays, without using color filters and typically have bandwidths in the hundreds of kHz region, meaning that high throughputs are possible with the help of digital equalizers [3]–[5].

Despite these advantages, SMOLEDs are most effectively processed via evaporation in high-vacuum chambers, that is less technologically appealing than solution-processing. A more suitable and attractive option is represented by PLEDs, which can instead be processed readily via a number of solution-based methods; thus potentially enabling ultra-low-cost thin film screens of individually addressable pixel matrices. Furthermore, PLEDs with active areas of a few μm^2 and bandwidths in excess of 60 MHz have been demonstrated [6], making them a serious competitor for a variety of intelligent display applications. Display technologies must be able to render a large range of visible wavelengths and as such require individual red, green and blue (RGB) pixels. Fortunately, there are an abundance

Manuscript received May 28, 2014; revised November 3, 2014; accepted March 10, 2015. Date of publication May 12, 2015; date of current version August 17, 2015. This work was supported by the EU COST Action IC1101, EU FP7 MC ITN GENIUS Grant number PITNCT2010-264694 and by the EPSRC (GR/S58416/01).

P. A. Haigh is with the Department of Electrical and Electronic Engineering, University College London, London WC1E 6BT, U.K., and also with the Faculty of Engineering, University of Bristol, Bristol BS8 1TR, U.K. (e-mail: paul.anthony.haigh@ieee.org).

F. Bausi and F. Cacialli are with the Department of Physics and Astronomy, University College London, London WC1E 6BT, U.K. (e-mail: f.bausi@ucl.ac.uk; f.cacialli@ucl.ac.uk).

H. Le Minh and A. Burton are with the Faculty of Engineering and Environment, Northumbria University, Newcastle upon Tyne NE1 8ST, U.K. (e-mail: hoa.le-minh@northumbria.ac.uk; andrew.burton@northumbria.ac.uk).

I. Papakonstantinou is with the Department of Electrical and Electronic Engineering, University College London, London WC1E 6BT, U.K. (e-mail: i.papakonstantinou@ucl.ac.uk).

W. O. Popoola is with the Institute for Digital Communications, School of Engineering, University of Edinburgh, Edinburgh EH9 3JL, U.K. (e-mail: w.popoola@ed.ac.uk).

Color versions of one or more of the figures in this paper are available online at http://ieeexplore.ieee.org.

Digital Object Identifier 10.1109/JSAC.2015.2432491

of polymers that emit (and absorb) in the visible range, with band gap energies between 1–4 eV [7], meaning this is also a straightforward task.

In this paper, we investigate the first key steps toward this goal and examine the individual communications performance of individual RGB pixels. The RGB pixels are produced using a constant device structure (to be detailed in Section II) and varying the emissive layer polymer between MDMO-PPV (red), F8BT (green) and F8:TFB:PFB (blue) (see below for full chemical definitions). The simultaneous transmission of different wavelengths is known as wavelength-division multiplexing (WDM) and is becoming increasingly popular in inorganic VLC systems as a means for increasing capacity through optically isolated parallel links. For instance, a transmission speed of 3.4 Gb/s was achieved in [8] using RGB wavelengths and the orthogonal frequency division multiplexing (OFDM) modulation format. In this paper, we adopt on-off keying (OOK) as the modulation format due to its simplicity of implementation in comparison to OFDM. It is commonly presumed that OFDM will offer an increase in spectral efficiency over OOK. While this is true for un-equalized OOK, literature has shown that using a digital equalizers (such as decision-feedback) with OOK and further orders of pulse amplitude modulation requires less signal-to-noise ratio (SNR) to achieve the same transmission speed [9], [10]. As a result a similar approach is adopted in this work. Artificial neural networks (ANNs), in particular the multi-layer perceptron (MLP) offers a further SNR gain over the decision-feedback equalizer [11] and hence are adopted instead. In this paper, we explore the potential toward WDM-PLED-VLC and experimentally found that the red and blue components can support up to 27.9 Mb/s and 18.6 Mb/s, respectively, and the green component can offer 8.4 Mb/s when using the MLP-ANN equalizer, representing a total potential data rate of 54.9 Mb/s. This is a substantial improvement over the current state-of-the-art literature, which reports 11.2 Mb/s using an F8:TFB:PFB device [3]. While this is the absolute maximum potential throughput for this type of system, it would be expected that a drop in throughput would be observed when simultaneous transmission of the wavelengths occurs. Without the equalizer we demonstrate that transmission speeds of 7 Mb/s, 4 Mb/s, and 2 Mb/s can be sustained for blue, red and green devices, respectively, and an overall transmission speed of 13 Mb/s, which represents a 10 Mb/s gain over the state of the art [3]–[5].

This paper is organized as follows. In Section II the production techniques used to process the PLEDs are outlined. In Section III the electrical characterization of the PLEDs is performed. Next, in Section IV the communications test setup and theoretical description of the equalizer is discussed. Finally, in Sections V and VI the results are discussed and the conclusions are drawn with a discussion of future outlook, respectively.

II. Polymer Light-Emitting Diode Processing

One of the main limitations of organic photonic devices is the polymer degradation mechanisms associated with contact with oxygen/water from air, which drastically limits performance and lifetime [12]. As a result, the PLEDs produced for this work are prepared in a nitrogen atmosphere and are encapsulated between two glass slides with an epoxy resin for utilization in air without any apparent degradation with time.

For preparation of all of the devices, a glass substrate is used with a pre-patterned ∼110 nm thick indium tin oxide (ITO) film as a transparent anode (Ossila Ltd) which allows six independent PLEDs. The ITO was cleaned with sonication in acetone and isopropanol and treated with oxygen plasma [13] in order to increase the work function and reduce the surface roughness [13], [14]. Afterwards, we deposited a hole-injection layer (40 nm) of PEDOT:PSS (Heraeus Clevios P VP AI 4083) via spin-coating (5000 rpm for 30 s in air). It consists of a water solution of poly(3,4-ethylenedioxythiophene) (PEDOT) doped with poly(styrenesulfonic acid) (PSS). The PEDOT:PSS blend has a relatively high conductivity (in the range of $0.2-2\times10^{-2}$ S/cm) and a work function of about 5.2 eV. It improves the hole-injection at the interface with the active layer. The samples are then annealed at 150 °C for 10 minutes in nitrogen atmosphere to remove water residues and improve the hole-injection performance. The general schematic of the PLEDs is shown in Fig. 1; while the emissive layer is different for device type as described individually as follows. The molecular structure of each polymer used is detailed inset in Fig. 1.

A. The red emissive layer consists of poly [2-methoxy-5-(3′,7′-dimethyloctyloxy)-1,4-phenylenevinylene] (MDMO-PPV) with an M_n of ∼23,000 g/mol (Sigma-Aldrich) deposited via spin coating from a 1% w/w (8.76 g/mL) solution in toluene.

B. The green photoactive polymer is poly[(9,9-di-*n*-octylfluorenyl-2,7-diyl)-*alt*-(benzo[2,1,3]thiadiazol-4,8-diyl)] (F8BT) with an M_n of 73,000 g/mol (American Dye Source). The layer was deposited via spin-coating from a 2% w/w (17.3 g/mL) solution in toluene.

C. The blue photoactive layer is a blend of three blue-emitting polymers: poly(9,9-dioctyluorene) (F8), (poly (9,9-dioctyluorene-*alt*-*N*-(4-butylphenyl)diphenylamine) (TFB) and poly(9,90-dioctyluorene-*alt*-bis-*N*,N_0-(4-butylphenyl)-bis-*N*,N_0-phenyl-1,4-phenylenediamine) (PFB) (American Dye Source) in a 1 : 2 : 2 ratio in a 2% w/w solution in mixed xylenes (Sigma-Aldrich).

For all device types, the photoactive layer was deposited via spin-coating at 2000 rpm for 60 s.

The red emissive polymer layers were also subject to thermal annealing that resulted in a higher bandwidth of the devices [4], [15]. We annealed the samples for 10 minutes at 150 °C (glass transition temperature is ∼75 °C for PPV derivative [16]). This effect could be explained with a thermally-induced reorganization of the MDMO polymer chains favoring the inter-chain interaction and hence determining a better charge transport [17]. The treatment also causes a partial, but acceptable, decrease in the luminance due to molecular aggregation. The blue and green devices were not annealed.

As a final step to complete all of the devices, a metallic cathode was deposited by evaporating a thin (30 nm) layer of calcium covered by a protective layer (150 nm) of aluminium.

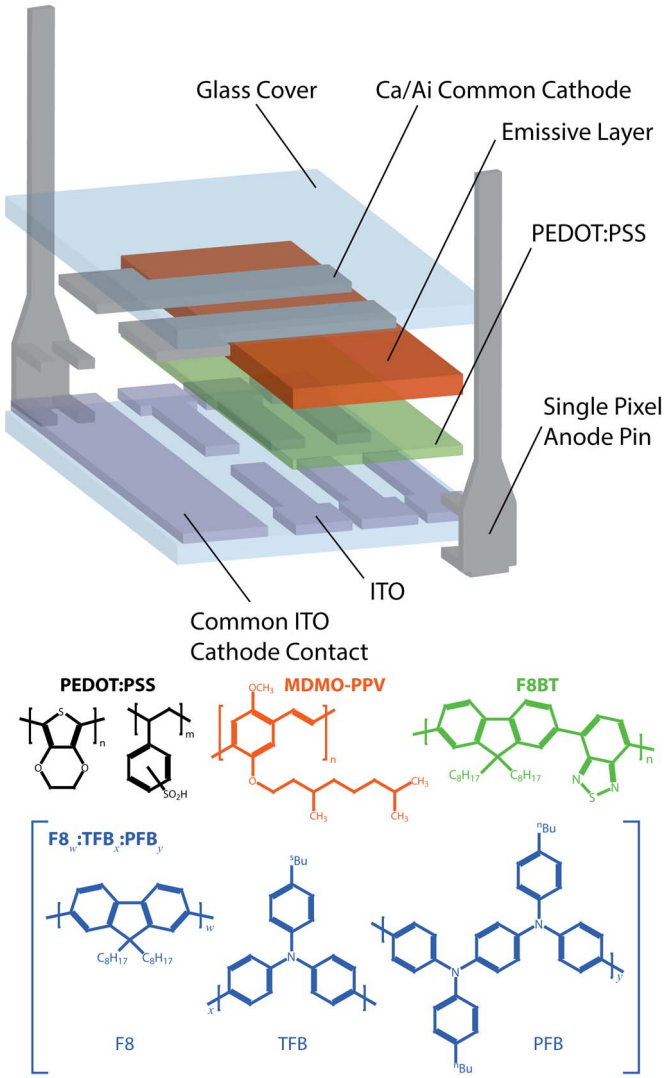

Fig. 1. An exploded schematic of the PLED used in this work; inset are the molecular structures of the polymer emissive layers.

Then we completed the encapsulation of the devices by applying a protective glass slide using a UV-hardened epoxy-glue (Ossila Ltd); curing is done with a low-power UV lamp (4 mW/cm^2) for 15 minutes in nitrogen.

III. PLED Electrical Characterisation

The normalized emission intensities are shown in Fig. 2. In clean WDM systems, it would be expected that the emission intensities would not overlap as heavily as with the polymers used here. For this reason to demonstrate a best-case performance, the RGB pixels are illuminated individually, thus avoiding interference introduced by crosstalk. The peak wavelengths for the RGB components are 480 nm, 538 nm and 598 nm, respectively and the blue component has a large spectral peak at 624 nm.

The measured DC current-luminance and current-voltage relationships (L-I-V) are shown in Fig. 3. The current was sourced by a Keithley 2400 current source which also measured the voltage across the diode. The luminance was measured

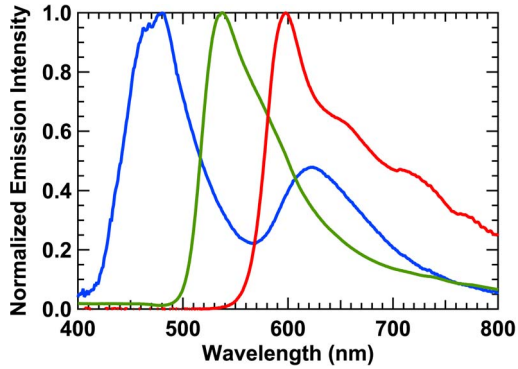

Fig. 2. Normalized emission intensity for the PLED pixels under test, with peak wavelengths of ~480 nm (blue), ~535 nm (green) and ~595 nm (red). The blue device also exhibits a peak at ~620 nm. Each device has a characteristic sharp cut-on wavelength and relaxed cutoff wavelength.

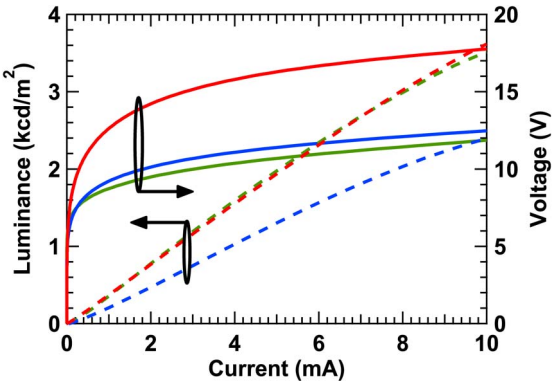

Fig. 3. The LIV relationships of each of the PLEDs; the solid lines correspond to the voltages and the dashed lines correspond to the luminances. Each device exhibits excellent linearity to avoid nonlinear impairmenets to the signals.

indirectly by converting the voltage output from a calibrated silicon photodetector using a Keithley 2000 digital multimeter. The L-I curves are sufficiently linear within the operating range (fitting curves are not shown for clarity; R^2 values are 0.998, 0.997, and 0.988 for RGB, respectively), thus signal clipping can be avoided. Furthermore, the system bandwidth is also controlled according to the current bias point due to presence of semiconductor charge traps, which are introduced at the processing time due to defects and impurities [18].

The charge traps have an associated time constant, which is itself proportional to the ratio of occupied/vacant traps. By increasing the injection current, the number of occupied traps increases; thus the associated time constant decreases. When all of the traps are occupied, the bandwidth becomes limited by the capacitive time constant as in inorganic devices. This mechanism has been described in the literature for both organic photodetectors (OPDs) [19], and more generally for organic layers, as in [20] to name just a few. We have therefore selected the bias currents with the following constraints; (*i*) so as to follow in the most linear region of the L-I response and (*ii*) for the bandwidth-limited by capacitance. More specifically, the operating points were therefore selected as; 8 mA AC, 6 mA DC for all the devices.

The measured bandwidths for the RGB pixels are shown in Fig. 4 and were measured using a Tektronix AFG2022B arbitrary function generator (AFG) and an Agilent MXA N9010A

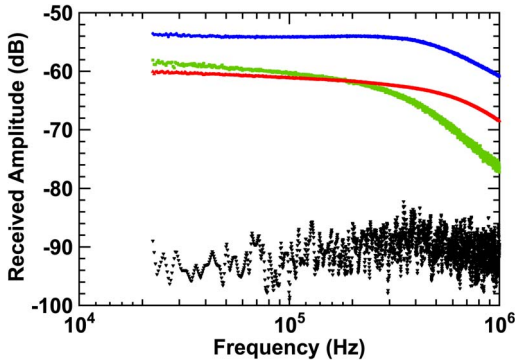

Fig. 4. Bandwidths of the PLEDs under test; measured by an Agilent MXA N9010A spectrum analyzer as 600 kHz (blue), 350 kHz (red) and 110 kHz (green).

electrical spectral analyser. The 3 dB bandwidths were measured as ∼350, 110 and 600 kHz for red, green and blue, respectively and the noise floor is also shown in black.

IV. Test Setup and Equalizer Under Test

The test setup is illustrated by the schematic block diagram in Fig. 5(a). A $2^{10}-1$ pseudorandom binary sequence (PRBS-10) is generated using MATLAB and loaded into the memory of the AFG using a LabVIEW script. The PRBS-10 data is passed through a unity height rectangular pulse shaping filter $p(t)$ and output to a single pixel via a current mirror driving circuit. Each pixel has an individual driving circuit that is tailored to the respective L-I-V relationships to enable the best possible performance.

The transmission distance is set to 0.05 m, consistent with the literature [3]–[5], because singular pixels of ∼3.5 mm^2 were used which have relatively low luminance. In order to improve this distance, matrices of pixels could be used, which will be implemented in our future work. When scaling up from a single pixel to multiple pixels, the performance of the diodes is not expected to vary. Reports in the literature show that the SNRs in VLC systems are dominated by the line-of-sight path between the transmitter and receiver [21]–[24] and the strongest diffuse component is at least 7 dB (electrical) lower than the line-of-sight component, thus meaning the multipath interference will have little effect [22]. Furthermore, the literature has shown that the bandwidth of a typical room is > 100 MHz, which is larger than the gross transmission speed reported in this work.

The optical power is absorbed and the photocurrent is amplified by a ThorLabs PDA36A packaged silicon photodetector with inbuilt transimpedance amplifier (10 dB, 5.5 MHz bandwidth). The continuous time photovoltage is sampled by a real time Agilent DSO9254A oscilloscope at a rate of $t = t_s$. The sampling rate $f_s = 1/t_s$ is set to a maximum of 10 S/sym and at least 10^7 samples were recorded leading to an uncoded bit error rate (BER) target of 10^{-6} in line with ITU specifications [25]. The discrete time signal is passed through a fourth order low-pass filter and the Q-factor is measured (not shown in Fig. 5(a)) to give a fast estimate of system performance. The signal is passed through a post emphasis circuit that consists of several high-pass filters of increasing order in parallel, added to the received signal path as shown in Fig. 5(b). The overall frequency response of the post-emphasis circuit can be represented with respect to the normalized cut-on frequency as follows:

$$y(f) = q(f) + \sum_{\rho=1}^{m} \frac{1}{\left[\sqrt{1+\left(\frac{f}{f_c}\right)^2}\right]^{\rho}} \tag{1}$$

Where m is the maximum order filter under test and f_c is the filter cut-on frequency and $q(f)$ is the frequency response of the received signal. Extensive studies not shown in this work have demonstrated theoretically and experimentally that a substantial improvement in Q-factor can be yielded by setting $m = 4$. While for $m > 4$ the improvement obtained is marginal. The filter weights are found by sweeping through a predetermined range of cut-on frequencies and measuring the Q-factor until a maximum value is found. The Q-factor is given by:

$$Q = \frac{\nu_H - \nu_L}{\sigma_H + \sigma_L} \tag{2}$$

where ν_H and ν_L are the high and low mean received voltages, respectively, and σ_H and σ_L are the high and low level standard deviations, respectively. Once the maximum value is found for each of the filters in the post-emphasis module, the filter coefficients are locked and the transmission occurs.

The post-emphasis circuit attempts to restore the attenuated high frequency components of the signal. The principle of operation of the proposed post-emphasis circuit is based on iteratively adjusting the weights of the filter based on the measured Q-factor at the output. Once the optimal filter is found, the signal is down-sampled using the integrate/dump method to maximize SNR. The system is then equalized, as will be discussed later and sliced by an average level threshold before comparison with the transmitted bits, symbol-by-symbol in a BER tester (BERT).

Inset in Fig. 5(a) are a photograph of the RGB devices, and the responsivity of the photodetector in the context of thenormalized emission intensities of the three devices. The responsivities (peak wavelengths) are 0.14 A/W (480 nm), 0.21 A/W (538 nm) and 0.27 A/W (598 nm), respectively. Obviously there is a significant difference between the responsivities of the blue/red components (around two times) and this will affect the link SNR. This is slightly compensated by the fact that the blue component has a large spectral peak, centerd at 624 nm (0.48 A/W).

A. Equalizer

The equalizer used in this work is an ANN based MLP, the structure of which is shown in Fig. 5(c).

The key difference between the MLP and other types of conventional equalizers such as decision feedback or linear feedforward is the overall operation. Conventional equalizers work on the principle of calculating the contribution of inter-symbol interference (ISI) from previous symbols on the current symbol. On the other hand, ANNs operate on the principle of classification; grouping received samples into classes based on a training sequence. This means that explicit calculation of the

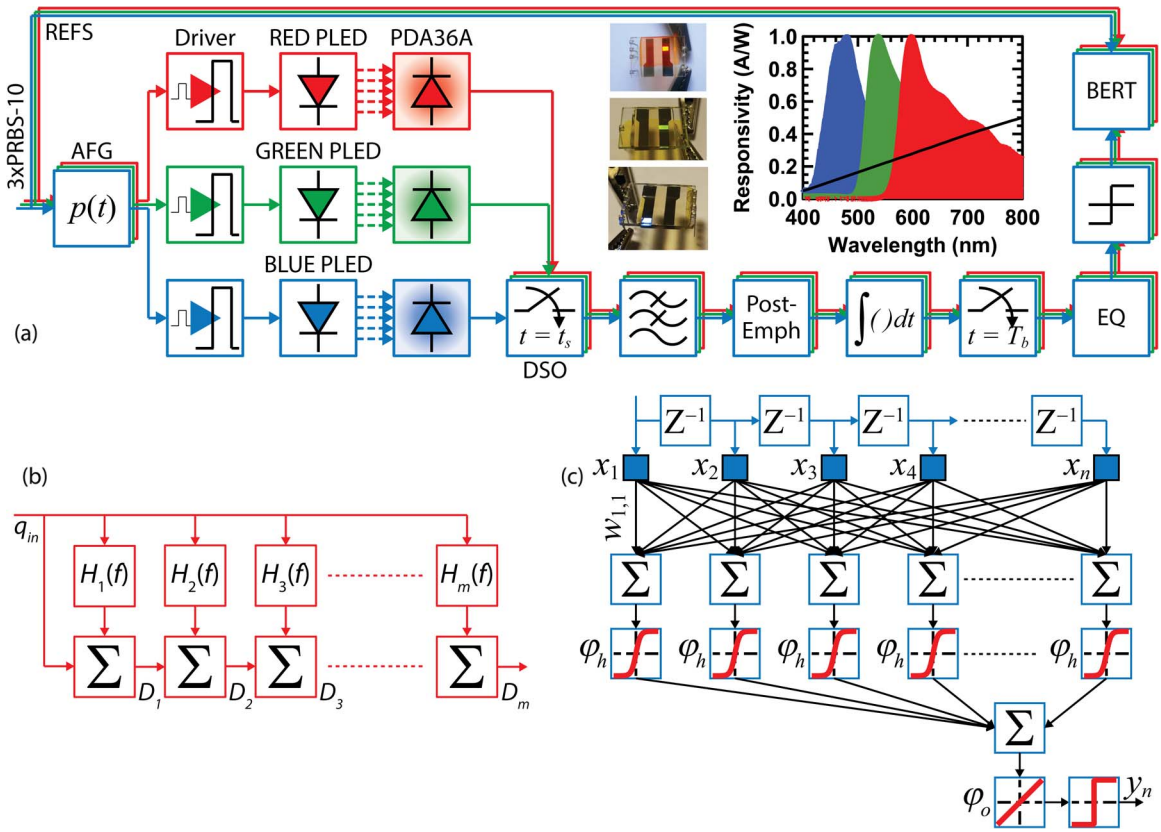

Fig. 5. Schematic block diagrams of (a) the system under test as described in the test; inset are top-view photographs of the three RGB PLEDs and the responsivity of the PD in the context of the emission spectra; (b) the post-empahsis module and (c) the equalizer under test.

ISI is not required and classification boundaries must instead be formed. The least complex digital implementation of the MLP is as a linear transversal filter (in opposition to a lattice), as with conventional equalizers. The MLP outperforms conventional equalizers such as linear and decision feedback equalizers [11], [26]. For further information on MLP, readers are encouraged to refer to [27]. The filter consists of N tapped delay inputs known as the observation vector $\mathbf{X} = [x_0, x_1, \ldots, x_N]$. Each input has an associated weight w_n as in conventional equalizers. The functional unit of the ANN is the neuron, which is where the processing happens, consisting of the sum of the weighted inputs and a (typically) nonlinear activation function (selected as log-sigmoid here) that allows computation of the filter output. Thus, the output of the filter is given as follows [28]:

$$y_n = \varphi\left(\sum_n w_n x_n\right) \tag{3}$$

where φ is the log-sigmoid activation function given by [27]:

$$\varphi = \frac{1}{1 + e^{-\beta\xi}} \tag{4}$$

where ξ is the weighted input and β is the slope parameter, set to unity in this work.

The MLP must be trained in order to be able to classify the input symbols. The most popular training method, also adopted here, is the Levenberg-Marquardt back propagation algorithm. In this algorithm, the ANN adjusts its weights in order to minimize the error cost function $E(n)$ as follows [28]:

$$E_n = \|d_n - y_n\|^2 \tag{5}$$

where d_n is the desired symbol value at sample n and y_n is the actual value. The Levenberg-Marquardt algorithm is an iterative procedure performing a gradient descent on E_n. The weights are updated as follows [28]:

$$w_{nj}(k+1) = w_{nj}(k) - \eta\frac{\partial E_n}{\partial w_{nj}(k)} \tag{6}$$

where w_{nj} is the weight between the interconnection of input x_n and neuron n_j. The number of neurons is set equal to the number of tapped inputs in order to provide a unity efficiency ANN [27]. To the best of our knowledge, there is no algorithm that describes the optimal number of neurons and tapped inputs and hence the best strategy is to start with a small network and add tapped inputs and neurons until the system performance is sufficient or the system limits are met. On the other hand, it can be advantageous to begin with a large network and prune it until the desired performance is found. Therefore, here we test a series of values as the number of neurons (and tapped inputs) in order to show the difference in performance. The values selected are $N = \{5; 10; 20; 30; 40\}$.

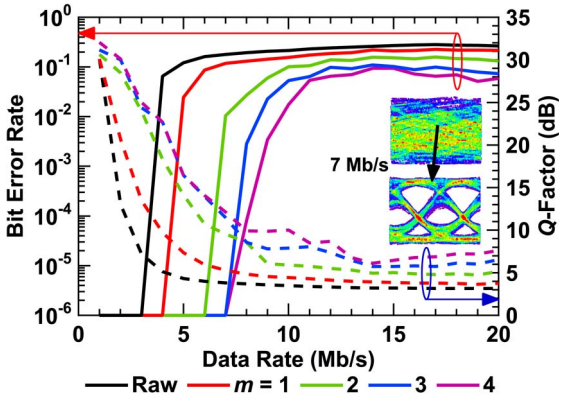

Fig. 6. Unequalized BER and Q-factor performance of the blue PLED; up to 7 Mb/s can be achieved when using the post-emphasis module in comparison to 3 Mb/s without it.

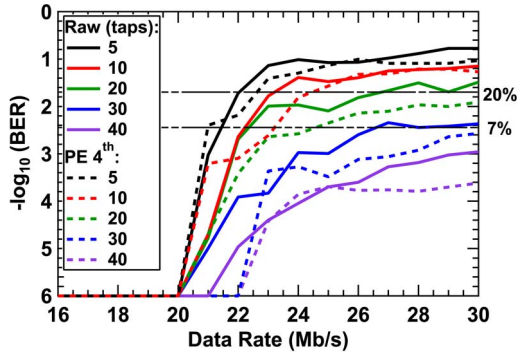

Fig. 7. Equalized BER performance of the blue PLEDs; up to 22 Mb/s can be achieved error free while up to 27.9 Mb/s can be sustained considering a 7% FEC limit.

V. Results and Discussion

The results will be presented in terms of individual wavelengths. The first type of devices to be discussed are the F8:TFB:PFB (blue) PLEDs because they offer best performance as will be shown. Subsequently MDMO-PPV (red) devices will be discussed followed by F8BT (green) devices.

A. BER Performance of F8:TFB:PFB Devices

The unequalized raw BER and Q-factor performance before and after the post-emphasis module for the blue devices are shown in Fig. 6.

It is clear that the post-emphasis module has a clear impact on the BER performance of the link as expected, improving the error free (at BER $= 10^{-6}$) transmission speed from 3 Mb/s up to 7 Mb/s using four filters in parallel. This is also represented by a substantial ~9 dB gain in Q-factor from 3.8 dB in the raw case to 12.2 dB in the post-emphasised case, as is reflected in the eye diagrams inset, which illustrate this improvement with a clear eye opening. The improvement can also be seen at 20 Mb/s, a transmission speed well outside of the modulation bandwidth, reducing the BER from ~0.4 in the raw case to $\sim 4 \times 10^{-2}$; or one order of magnitude. On the other hand, this BER is not sufficiently low to apply forward error correction (FEC) codes, which require a maximum BER of 3.6×10^{-3} or 2×10^{-2} considering a 7% or 20% overhead, respectively [3]. Due to space constraints inside Fig. 6 the legend is shown below. It should be noted that this is a remarkable transmission speed to achieve, representing a net gain of 133% in comparison with the state-of-the-art unequalized error free data rate reported in the literature (3 Mb/s), which was achieved using both MDMO-PPV and F8:TFB:PFB PLEDs [3]–[5].

The ANN equalized BER performance before (solid lines) and after the post-emphasis (dashed lines) module are both shown in Fig. 7. Recall that the number of taps is set equal to the number of neurons in the equalizer for full efficiency and ranges within the set $N = \{5; 10; 20; 30; 40\}$. The two most important results in Fig. 7 are as follows; (*i*) error free transmission (BER $= 10^{-6}$) can be supported using $N = \{30; 40\}$ taps if the pre-emphasis module is included. If it is not, transmission speeds are limited to 21 Mb/s for $N = 40$ and 20 Mb/s for $N = \{5; 10; 20; 30\}$; (*ii*) considering the 7% FEC limit, gross transmission speeds up to 30 Mb/s are readily available in this link either using the post-emphasis module and $N = \{30; 40\}$ or without the post-emphasis module and $N = 40$, leading to a net transmission speed of 27.9 Mb/s after deduction of the 7% overhead.

It should be noted that both the 22 Mb/s uncoded error free and 27.9 Mb/s FEC coded transmission speeds using the ANN equalizer reported here represent a significant improvement over the existing literature at the time of writing. The previous reported work [3] has maximum uncoded and FEC coded transmission speeds of 10 Mb/s and 11.2 Mb/s, respectively for F8:TFB:PFB PLEDs [3], therefore an improvement of 120% and 149%, respectively, can be observed.

For $N = \{5; 10; 20\}$, the system only sustains an error free transmission speed up to 20 Mb/s as mentioned. For $N = 20$ taps and considering the 7% FEC with and without the post-emphasis module, gross (net) transmission speeds of 25 (23.25) and 22 (20.36) Mb/s can be achieved, respectively which demonstrate a considerable reduction over $N = \{30; 40\}$ and are thus suboptimal. Considering the 20% FEC, gross (net) transmission speeds of 30 (24) and 26 (20.8) Mb/s can be sustained with and without the post-emphasis module, respectively. For $N = 10$ and considering the 7% FEC limit, gross (net) transmission speeds of 23 (21.39) Mb/s and 22 (20.46) Mb/s can be supported, offering slight gains of up to ~1.4 Mb/s over the uncoded error rate. The available gross (net) transmission speeds considering the 20% FEC are 23 (18.4) Mb/s and 24 (19.2) Mb/s, actually causing a reduction in available capacity over the uncoded rate. Similarly for $N = 5$ the available transmission speeds drop below those of the uncoded data rates in all configurations. To provide an illustrative example of the improvement between the worst and best cases, the first 1×10^5 samples at the output of the ANN equalizer are shown for a transmission speed of 30 Mb/s in Fig. 8 for the system with an ANN equalizer using 5 taps (blue) and 40 taps with the post-emphasis module (black). The vertical red line indicates the length of the training sequence (1×10^4) and hence the pattern slightly degrades after this point due to the high noise level at 30 Mb/s. It is clearly possible to determine two definite signal levels for thresholding in the best case of $N = 40$ taps

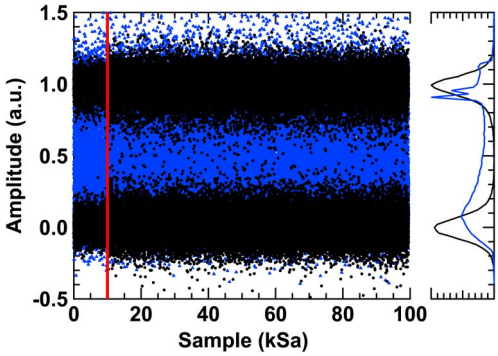

Fig. 8. The equalizer output for the first 10^5 samples (including 10^4 training samples) indicating the substantial classification improvement between $N = 40$ (black) and 5 (blue) taps/neurons.

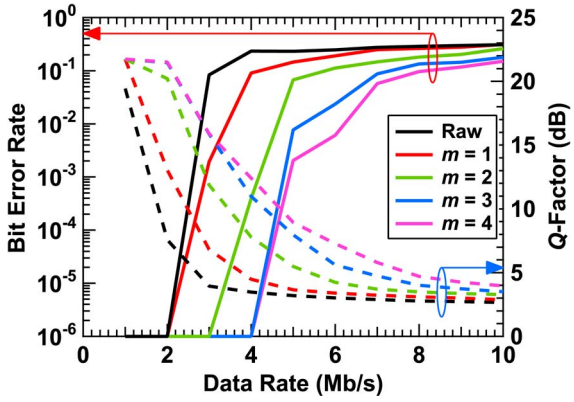

Fig. 9. Unequalized BER and Q-factor performance of the red devices; up to 4 Mb/s can be achieved with the post-emphasis module in comparison to 2 Mb/s without it.

and the post-emphasis, and in the worst case, with $N = 5$ taps, impossible to define any level.

B. BER Performance of MDMO-PPV Devices

Similarly to the F8:TFB:PFB devices the raw, unequalized BER and Q-factor performance of the MDMO-PPV devices are first shown in Fig. 9 with and without the post-emphasis module.

Once more it is clear that the post-emphasis module has a large impact on the available transmission speed; improving it from 2 Mb/s without the module to 4 Mb/s with a 4$^{\text{th}}$ order module, a 100% increase. However, in comparison to the previous devices, which showed an improvement of ~4 dB at 20 Mb/s, using the module with MDMO-PPV devices at high transmission speeds provides a substantially lower improvement. Only an additional ~1 dB in Q-factor is available at 10 Mb/s, which reduces further at higher transmission speeds. Thus it can be inferred that the module will have little impact at transmission speeds > 10 Mb/s while adding additional complexity to the system, which proved to be the case after extensive tests, hence the post-emphasis module is not used for these devices.

In terms of the ANN equalized BER performance, which is shown in Fig. 10, error free (at BER = 10^{-6}) is available up to transmission speeds of 18 Mb/s using $N = 40$ taps and

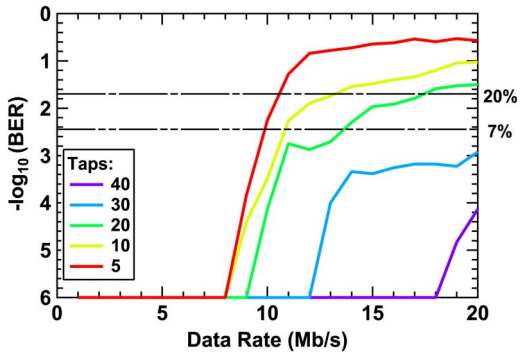

Fig. 10. As the post-emphasis module has little effect in the red system for transmission speeds >10 Mb/s, it is not considered here; transmission speeds up to 18 Mb/s can be supported with $N = 40$ taps in comparison to 8 Mb/s with $N = 5$ taps.

neurons. When considering the previously mentioned FEC limits, a transmission speed of 20 Mb/s is available with 40 taps, leading to an overall useful data rate of 18.6 Mb/s and a slight improvement over the error free rate.

For $N = 30$ the error free transmission speed is severely reduced to 12 Mb/s indicating that the ISI spans over 30–40 symbols in this link. Interestingly, for $N = 30$ the 7% FEC limit is never reached, meaning a transmission speed of 18.6 Mb/s can also be realized with 10 taps fewer, leading to a complexity advantage. If the number of taps is reduced to $N = 20$ the transmission speed is reduced below 10 Mb/s for the first time in this link to 9 Mb/s. On the other hand, at the 7% FEC limit a data rate of 14 Mb/s (gross) and 13.02 Mb/s (net) can be attained while for the 20% limit a data rate of 17 Mb/s (gross) and 13.6 Mb/s (net) is readily available. Finally, for $N = \{10; 5\}$ the error free data rate is further reduced to 8 Mb/s. Considering $N = 10$ and the 7% and 20% FEC limits, net data rates of 10.23 and 10.4 Mb/s are available. Finally, for $N = 5$, the rates are both reduced below 10 Mb/s for the 7% and 20% FEC to 9.3 Mb/s and 8 Mb/s, respectively.

C. BER Performance of F8BT Devices

Finally, the green devices will be discussed. The raw BER and Q-factor performance is shown in Fig. 11. For the F8BT devices the post-emphasis module does not cause any improvement in Q-factor or BER. The reason for this is due to the slow rise time of the PLEDs which is the major restriction of the link. The driving circuit was tested without the PLED and it was found to be free of a bandwidth limitation for the frequencies under test and hence it is inferred that the slow rise time is caused by the device itself rather than an external influence. The link is available error free (BER = 10^{-6}) up to 2 Mb/s, a significant reduction in comparison to the F8:TFB:PFB and MDMO-PPV devices due to the lower bandwidth/slow rise time.

Therefore, the total error free link performance can be given by the sum of the three links, giving the maximum performance for each device and hence the maximum total performance of the link. The total error free transmission speed readily available is 13 Mb/s, comprised of 7 Mb/s from the F8:TFB:PFB

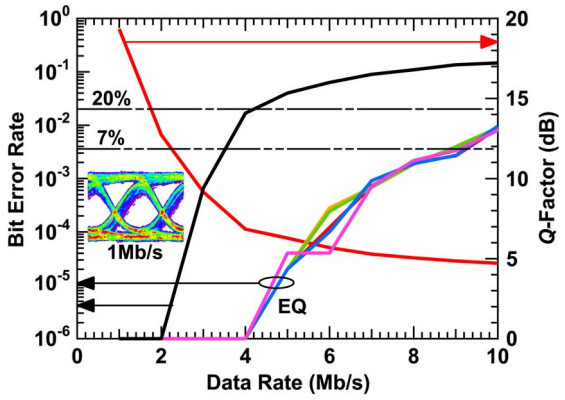

Fig. 11. Unequalized (black) BER and Q-factor performance of the green link; only 2 Mb/s can be recovered with no improvement evident from the post-emphasis module due to the slow rise time of the device. Also, shown is the ANN equalized performance (labeled EQ) for all values of N; the available data rate is independent of the number of neurons due to the low bandwidth of the link and low SNR.

devices, 4 Mb/s from the MDMO-PPV devices and 2 Mb/s from the F8BT devices. This is sufficient capacity to support an Ethernet link in real time without any equalization methods for the first time, which we will implement in our future work. Furthermore, as mentioned, the state-of-the-art unequalized transmission speed is reported at 3 Mb/s [3]–[5], so the parallel link reported here could supply an additional 10 Mb/s, or an increase of 333% which is remarkable.

The ANN equalized performance for the F8BT devices is also shown in Fig. 11 which shows the error free link capacity can be improved to 4 Mb/s for all values of N. This is substantially lower than has been demonstrated in the previous devices. The reason for this is twofold; (*i*) the bandwidth is at least half of the other two devices (110 kHz in comparison to 350 kHz (red) and 600 kHz (blue)); (*ii*) therefore the system SNR descends into the noise floor at a lower frequency. It is well known that equalizers cannot equalize uncorrelated, unbounded noise such as Gaussian noise and therefore the equalizer fails. Thus the total potential error free transmission speed available on aggregate from the link is 44 Mb/s, which is more than four times higher than the state-of-the-art reported in the literature (10 Mb/s [3]).

On the other hand, there is an improvement in transmission speed when considering the 7% FEC BER limit. A gross transmission speed of 9 Mb/s can be sustained by the link, leading to a net data rate of ∼8.4 Mb/s. Thus, the aggregate capacity of the link considering a 7% FEC is given as 54.9 Mb/s, representing approximately a fivefold gain over the state-of-the-art in the literature of 11.2 Mb/s [3], which is remarkable. It should be noted that the 44 and 54.9 Mb/s data rates are only available when each device is used independently. Cross-talk or inter-channel interference will cause degradation to these rates when simultaneous operation is performed, which will be investigated in our future work.

VI. Conclusion

In this paper, we have demonstrated a system of RGB PLEDs with potential toward implementing a ∼55 Mb/s PLED-VLC link. In order to achieve this we used three separate pixels of individual wavelengths and a high performance artificial neural network equalizer. This is an important result for the research community; however there are still key research challenges that remain. The most important of which is that when each component of the link is active simultaneously there will be a problem with inter-channel interference, or crosstalk. It would be expected that the green component of the link would most severely affected by the crosstalk due to high interference from both the red and blue components. In order to overcome this, either color filters or wavelength selective photodetectors can be used at the cost of SNR. Therefore, we propose in our future work to thoroughly investigate this challenge and analyse the performance in comparison to this link, which provides the best possible performance of such a link without considering crosstalk.

Acknowledgment

Franco Cacialli is a Royal Society Wolfson Research Merit Award holder.

References

[1] R. Das and P. Harrop, "Organic & printed electronics—Forecasts, players & opportunities 2007–2027," IDTechEx, Cambridge, U.K., Rep., 2010.
[2] L. Hanzo *et al.*, "Wireless myths, realities, and futures: From 3G/4G to optical and quantum wireless," in *Proc. IEEE*, vol. 100, no. Special Centennial Issue, pp. 1853–1888, May 2012.
[3] P. A. Haigh *et al.*, "A 10 mb/s visible light communication system using a low bandwidth polymer light-emitting diode," in *Proc. IEEE CSNDSP*, Jul. 2014, pp. 999–1004.
[4] P. A. Haigh *et al.*, "Visible light communications: Real time 10 Mb/s link with a low bandwidth polymer light-emitting diode," *Opt. Exp.*, vol. 22, no. 3, pp. 2830–2838, 2014.
[5] P. A. Haigh *et al.*, "Next generation visible light communications: 10 Mb/s with polymer light-emitting diodes," in *Proc. Opt. Fiber Commun. Conf.*, 2014, pp. 1–3.
[6] I. A. Barlow, T. Kreouzis, and D. G. Lidzey, "High-speed electroluminescence modulation of a conjugated-polymer light emitting diode," *Appl. Phys. Lett.*, vol. 94, no. 24, pp. 243 301–243 303, Jun. 2009.
[7] J. Clayden, N. Greeves, and S. Warren, *Organic Chemistry*. Oxford, U.K.: Oxford Univ. Press, 2012.
[8] G. Cossu, A. M. Khalid, P. Choudhury, R. Corsini, and E. Ciaramella, "3.4 Gbit/s visible optical wireless transmission based on RGB LED," *Opt. Exp.*, vol. 20, no. 26, pp. B501–B506, Dec. 2012.
[9] D. J. F. Barros and J. M. Kahn, "Comparison of orthogonal frequency-division multiplexing and on-off keying in amplified direct-detection single-mode fiber systems," *J. Lightw. Technol.*, vol. 28, no. 12, pp. 1811–1820, Jun. 2010.
[10] D. J. F. Barros, S. K. Wilson, and J. M. Kahn, "Comparison of orthogonal frequency-division multiplexing and pulse-amplitude modulation in indoor optical wireless links," *IEEE Trans. Commun.*, vol. 60, no. 1, pp. 153–163, Jan. 2012.
[11] K. Burse, R. N. Yadav, and S. C. Shrivastava, "Channel equalization using neural networks: A review," *IEEE Trans. Syst., Man, Cybern. C, Appl. Rev.*, vol. 40, no. 3, pp. 352–357, May 2010.
[12] R. H. Friend *et al.*, "Electroluminescence in conjugated polymers," *Nature*, vol. 397, no. 6715, pp. 121–128, 1999.
[13] T. M. Brown and F. Cacialli, "Contact optimization in polymer light-emitting diodes," *J. Polymer Sci. B, Polymer Physics*, vol. 41, no. 21, pp. 2649–2664, Nov. 2003.
[14] N. Johansson *et al.*, "A study of the ITO-on-PPV interface using photoelectron spectroscopy," *Synthetic Metals*, vol. 92, no. 3, pp. 207–211, 1998.
[15] S. T. Le *et al.*, "10-Mb/s visible light transmission system using a polymer light-emitting diode with orthogonal frequency division multiplexing," *Opt. Lett.*, vol. 39, no. 13, pp. 3876–3879, 2014.
[16] M. Kemerink *et al.*, "Substitution and preparation effects on the molecular-scale morphology of PPV films," *Macromolecules*, vol. 38, no. 18, pp. 7784–7792, 2005.

[17] Z. E. Lampert, S. E. Lappi, J. M. Papanikolas, C. Lewis Reynolds, Jr, and M. O. Aboelfotoh, "Morphology and chain aggregation dependence of optical gain in thermally annealed films of the conjugated polymer poly[2-methoxy-5-(2-ethylhexyloxy)-p-phenylene vinylene]," *J. Appl. Phys.*, vol. 113, no. 23, 2013, Art. ID. 233509.
[18] H. T. Nicolai *et al.*, "Unification of trap-limited electron transport in semiconducting polymers," *Nat. Mater.*, vol. 11, no. 10, pp. 882–887, Oct. 2012.
[19] F. Arca *et al.*, "Interface trap states in organic photodiodes," *Sci. Rep.*, vol. 3, p. 1324, 2013.
[20] J. M. Montero, J. Bisquert, G. Garcia-Belmonte, E. M. Barea, and H. J. Bolink, "Trap-limited mobility in space-charge limited current in organic layers," *Organic Electron.*, vol. 10, no. 2, pp. 305–312, Apr. 2009.
[21] M. Hoa Le *et al.*, "High-speed visible light communications using multiple-resonant equalization," *IEEE Photon. Technol. Lett.*, vol. 20, no. 14, pp. 1243–1245, Jul. 2008.
[22] L. Zeng *et al.*, "High data rate multiple input multiple output (mimo) optical wireless communications using white LED lighting," *IEEE J. Sel. Areas Commun.*, vol. 27, no. 9, pp. 1654–1662, Dec. 2009.
[23] A. M. Khalid, G. Cossu, R. Corsini, P. Choudhury, and E. Ciaramella, "1-Gb/s transmission over a phosphorescent white LED by using rate-adaptive discrete multitone modulation," *IEEE Photon. J.*, vol. 4, no. 5, pp. 1465–1473, Oct. 2012.
[24] M. Hoa Le *et al.*, "100-Mb/s NRZ visible light communications using a postequalized white LED," *IEEE Photon. Technol. Lett.*, vol. 21, no. 15, pp. 1063–1065, Aug. 2009.
[25] I. T. Sector, "Error performance parameters and objectives for international constant bit rate digital paths at or above the primary rate," International Telecommunication Union (ITU), Geneva, Switzerland, ITU-T Study Group 131WP-6, ITU-T recommendation G.826, 1993.
[26] A. Zerguine, A. Shafi, and M. Bettayeb, "Multilayer perceptron-based DFE with lattice structure," *IEEE Trans. Neural Netw.*, vol. 12, no. 3, pp. 532–545, 2001.
[27] S. Haykin, *Neural Networks: A Comprehensive Foundation*, 2nd ed. New Jersey, NJ, USA: Prentice-Hall, 1998.
[28] P. A. Haigh *et al.*, "Exploiting equalization techniques for improving data rates in organic optoelectronic devices for visible light communications," *J. Lightw. Technol.*, vol. 30, no. 19, pp. 3081–3088, Oct. 2012.

Paul Anthony Haigh received the B.Eng.(Hons.) degree in communications engineering and the Ph.D. degree in the area of organic visible light communications from Northumbria University, Newcastle upon Tyne, U.K., in 2010 and 2014, respectively. Between 2010 and 2011, he held the prestigious Marie Curie Fellowship at the European Organization for Nuclear Research (CERN), where he worked on the optoelectronic links in Large Hadron Collider experiments. He is currently a Research Associate with the High Performance Networks Group, University of Bristol, Bristol, U.K., working on the EPSRC TOUCAN project. He has authored or coauthored over 30 scholarly articles, including over 16 articles in high-ranking journals such as the IEEE JOURNAL ON SELECTED AREAS IN COMMUNICATIONS, the *IEEE Wireless Communications Magazine*, *Optics Express*, the *IEEE Communications Magazine*, and the *IEEE/OSA Journal of Lightwave Technology*. His research is focused on real-time, seamless, transparent, and programmable interfaces between wired and wireless multitechnology networks.

Francesco Bausi is currently working toward the Ph.D. degree at the Centre for Nanotechnology, University College London, London, U.K. He works on plastic electronics, particularly on innovative applications of polymer light-emitting diodes and new materials for optoelectronics such as graphene-based transparent conductive thin films.

Hoa Le Minh has been a Senior Lecturer since 2010 and a Program Leader of electrical and electronics engineering since 2013 with Northumbria University, Newcastle upon Tyne, U.K. Prior to joining Northumbria University, he was a Researcher at Siemens AG, Munich, Germany, in 2002 and at the University of Oxford, Oxford, U.K., in 2007. His research areas are optical communications, visible light communications, and smartphone technology, in which he has authored or coauthored over 100 papers in the refereed journals and conferences. Mr. Le Minh serves as the Vice-Chairman of the IEEE Communications Chapter of the U.K. and Ireland. He is also a Guest Editor of IET and ETT journals.

Ioannis Papakonstantinou received the Ph.D. degree in polymer optical interconnects from University College London (UCL), London, U.K., in 2008. In 2008, he joined Sharp Laboratories of Europe as a Research Associate. While at Sharp, he received training on nanoimprint lithography, the subject of his proposed work in this proposal, and specialized in subwavelength structures to improve the energy efficiency, uniformity, and brightness of liquid crystal displays. Together with his colleagues at Sharp, he filed and was awarded five patents on the design and fabrication of antireflection coatings, nonabsorbing polarizers, color-separating gratings, and light in-coupling and out-coupling structures for backlights, all made by NIL. He is currently a Lecturer with the Department of Electronic and Electrical Engineering, UCL, where he leads a team of six Ph.D. students as Principal and Second Supervisor. Prior to joining UCL, in 2009–2011, he was with the Physics Department at the European Organization for Nuclear Research (CERN), where he developed optical network topologies for the distribution of time, trigger, and control signals in the Large Hadron Collider. He has almost ten years of experience in optical components made of polymers. His research interests lie in the areas of nanophotonics for renewable energy, medical equipment, and ICT applications.

Wasiu O. Popoola received the bachelor's degree (with first-class honors) in electronic and electrical engineering from Obafemi Awolowo University, Ife, Nigeria, and the M.Sc. and Ph.D. degrees from Northumbria University, Newcastle upon Tyne, U.K. He is currently a Chancellor's Fellow with the Institute for Digital Communications, The University of Edinburgh, Edinburgh, U.K, where he was a Research Fellow in visible light communications from March 2010 to June 2012. Previously, he was a Lecturer of electronic engineering at Glasgow Caledonian University, between August 2012 and December 2014. He has authored or coauthored over 60 journal articles/conference papers/patent, and over six of those are invited papers (see: http://goo.gl/JdCo3R). He has coauthored *Optical Wireless Communications: System and Channel Modelling with MATLAB* (CRC, 2012). He was a recipient of the 'Xcel Best Engineering and Technology Student of the Year in 2009 during his Ph.D. studies.

Andrew Burton received the B.Eng.(Hons.) degree, the M.Sc. degree (with distinction), and the Ph.D. degree in visible light communications from Northumbria University Northumbria, U.K. His research interests focus on electronics, optical communications, and visible light communications, in which he has 19 journal/conference publications. He is currently an Associate Lecturer with Northumbria University, where, in July 2015, he will be involved in a collaboration between Northumbria University and the European Space Agency to develop a simulation package for ground-to-space and space-to-ground free-space optical communications.

Franco Cacialli received the bachelor's degree and the Ph.D. degree in electronic engineering from the University of Pisa, Pisa, Italy. Since 2005, he has been a Professor of physics in the London Centre for Nanotechnology and the Department of Physics and Astronomy at University College London, London, U.K, where he was a Lecturer in 2001–2003 and then a Reader in 2003–2004. After postdoctoral work at Cambridge, he became a Royal Society University Research Fellow (1996–2004), first at Cambridge (until 2001). He coordinated an 11-partner Marie Curie Research Training Network dedicated to investigation of threaded molecular wires (THREADed Molecular wIres as supramoLecularly engineered muLtifunctional materials, www.threadmill.eu) and currently coordinates a new European Training Network dedicated to exploitation of supramolecular materials for photonics (SupramolecularlY eNgineered arCHitectures for optoelectRonics and photONICS, http://synchronics-etn.eu). He has (co)authored over 250 publications and six patents. He has also coedited (with P. Samori, Strasbourg) *Functional Supramolecular Architectures* (Wiley, 2010). His research interests focus on the physics and application of organic semiconductors (OS) to photovoltaic/light-emitting diodes and to field-effect transistors, with particular attention to the electronic properties of the electrode-semiconductors interface, an issue of fundamental importance in virtually all device applications. His research interests also include supramolecular architectures for the control and tailoring of intermolecular interactions, and thus of OS photophysics, and high-resolution nanolithography by means of the scanning near-field optical microscope or the scanning thermal microscope. He is a Fellow of the Institute of Physics (FinstP). He has been elected to a Fellowship of the American Physical Society in 2009. He is a recipient of a Royal Society Wolfson Research Merit Award (2015–2019).